Theoretical study of *K*-shell excitations in formaldehyde

A. B. Trofimov, T. E. Moskovskaya, and E. V. Gromov
Laboratory of Quantum Chemistry, Computer Center, Irkutsk State University, 664003 Irkutsk, Russian Federation

H. Köppel and J. Schirmer
Theoretische Chemie, Physikalisch-Chemisches Institut, Universität Heidelberg, Im Neuenheimer Feld 229, D-69120 Heidelberg, Germany

(Received 7 December 2000; published 11 July 2001)

The C 1*s* and O 1*s* excitation of formaldehyde (H_2CO) has been studied within an *ab initio* framework. The second-order algebraic-diagrammatic construction [ADC(2)] polarization propagator method has been used to calculate energies and oscillator strengths of the electronic transitions. For selected C 1*s* excited states also multireference configuration-interaction (MRCI) calculations were performed. The vibrational excitations accompanying the electronic transitions have been studied using a linear vibronic coupling model. The theoretical C 1*s* and O 1*s* spectra are in excellent qualitative agreement with high-resolution *K*-shell photoabsorption measurements. The present results support the previous assignments of the C 1*s* spectrum, while they revise the interpretation of the O 1*s* spectrum above 537 eV. In contrast to the C 1*s* case, the main photoabsorption intensity in the O 1*s* spectrum is due to *nd* rather than to *np* Rydberg excitations. For the two lowest singlet excited states, that is, the $^1B_1(\mathrm{C}\,1s\rightarrow\pi^*)$ single excitation and the $^1B_2(\mathrm{C}\,1s,n\rightarrow\pi^{*2})$ double excitation, we find vibronic interaction with the $^1A_1(\mathrm{C}\,1s\rightarrow 3s)$ and $^1A_2(\mathrm{C}\,1s\rightarrow 3d)$ Rydberg states via the ν_4 out-of-plane bending mode. In addition, the $^1B_2(\mathrm{C}\,1s,n\rightarrow\pi^{*2})$ and the $^1A_1(\mathrm{C}\,1s\rightarrow 3s)$ states interact via the ν_5 mode. The vibronic coupling leads to a complex spectral pattern in the low-energy part of the C 1*s* excitation spectrum, allowing one to interpret the finer details of the experiment.

DOI: 10.1103/PhysRevA.64.022504 PACS number(s): 31.10.+z, 33.20.Rm, 33.20.Tp

I. INTRODUCTION

The core-electron excitation in H_2CO has been studied in the past both experimentally [1,2] and theoretically [3–5]. Hitchcock and Brion [1] recorded C 1*s* and O 1*s* electron-energy-loss spectra of H_2CO for a wide range of excitation energies and determined positions and intensities of many electronic bands below the respective ionization thresholds. A subsequent theoretical study of vertical excitation energies and oscillator strengths [3] confirmed the assignments of many low-lying *K*-shell transitions given by Hitchcock and Brion [1] and discussed the basic physical effects governing core-electron excitation in H_2CO. An interesting finding of the latter work is that already the second transition in the C 1*s* spectrum is a double or ''two-particle–two-hole'' $(2p\text{-}2h)$ excitation of the type $\mathrm{C}\,1s,n\rightarrow\pi^{*2}(^1B_2)$. The advent of the soft-x-ray synchrotron-radiation sources has made possible very detailed studies of the *K*-shell excitations in molecules (see, e.g., Refs. [2,6–10]). A high-resolution K-shell photoabsorption study of H_2CO was performed by Remmers *et al.* [2]. This study yielded a wealth of previously inaccessible information, concerning especially the effects of nuclear motion accompanying electronic transitions. Many important results of this work are still not fully understood and await theoretical analysis. Recently Nooijen and Bartlett [4] and Fronzoni *et al.* [5] presented computations of *K*-shell excitation in H_2CO. However, the latter studies were primarily devoted to discussing methodological aspects of the computational schemes rather than to analyzing spectroscopic issues. In view of the present status, a thorough theoretical reinvestigation of *K*-shell electron excitation in the prototypical H_2CO molecule intended here should be both timely and desirable. In the work of Remmers *et al.* [2] a number of previously unresolved *K*-shell Rydberg excitations of H_2CO were identified and assigned. Since most of their assignments were made by analogy with the CO molecule [6], a verification based on *ab initio* results should be of interest. In particular, some of the earlier assignments of *K*-shell Rydberg excitations in H_2CO need to be reviewed on the grounds of reliable theoretical results. In Refs. [1–5] the C 1*s* and O 1*s* Rydberg spectra are interpreted in an essentially similar way, although the corresponding spectral profiles appear to be quite distinct, as can be seen already in the low-resolution spectra of Hitchcock and Brion [1]. This seems to indicate significant differences in the C 1*s* and O 1*s* Rydberg series, which apparently have been overlooked before. Here the previous theoretical studies [3–5] are not conclusive, because due to the lack of diffuse *d*-type basis functions a satisfactory description of the Rydberg manifolds was not achieved.

The high spectral resolution in the work of Remmers *et al.* [2] poses the challenging task of assigning the observed vibrational structure. In many cases there applies a simple Franck-Condon type of analysis of the totally symmetric vibrational modes $\nu_1-\nu_3$ as used by Remmers *et al.* [2]. However, this approach depends on the actual spectral resolution and becomes less reliable at higher excitation energies, where the electronic bands are overlapping. Also, some ambiguities concerning the geometrical parameters of core excited H_2CO have not fully been resolved in the work of Remmers *et al.* [2].

According to the results of a previous theoretical study [11] on the structure and stability of H_2CO in the lowest $^1B_1(\mathrm{C}\,1s\rightarrow\pi^*)$, $^1B_2(\mathrm{C}\,1s,n\rightarrow\pi^{*2})$, and $^1A_1(\mathrm{C}\,1s\rightarrow 3s\text{-}a_1)$ states [further also referred to as $^1B_1(\pi^*)$, $^1B_2(2p\text{-}2h)$, and $^1A_1(3s)$ states], vibronic coupling effects

should play an important role in the corresponding transitions. This is suggested by the finding that for both the $^1B_1(\pi^*)$ and the $^1B_2(2p\text{-}2h)$ states there is a double-well potential-energy surface (PES) with respect to the out-of-plane bending vibrational coordinate ν_4. Strong vibronic activity of the ν_4 mode should therefore be expected. Within the linear vibronic coupling (LVC) model the interaction via the $\nu_4(b_1)$ mode is likely to take place between the $^1B_1(\pi^*)$ and $^1A_1(3s)$ states and between the $^1B_2(2p\text{-}2h)$ and $^1A_2(3d)$ states. As suggested in Ref. [11], there is also the possibility of interaction between $^1B_2(2p\text{-}2h)$ and $^1A_1(3s)$ states *via* one of the b_2 modes (ν_5 and ν_6). The study of vibronic coupling effects in the lowest singlet C $1s$ excited states should help to clarify experimental findings such as the unusual isotopic effect on the position and width of the C $1s\rightarrow\pi^*(^1B_1)$ and C $1s\rightarrow 3s(^1A_1)$ transitions and the large width of the C $1s\rightarrow 3s(^1A_1)$ band. Since the intensity borrowing is a characteristic feature of vibronic coupling, a careful treatment of vibronic effects is quite important for the question of observability of the C $1s,n\rightarrow\pi^{*2}(^1B_2)$ transition in the optical absorption spectrum.

In the present paper we report on recent computations of electronic transitions and their vibrational structure in H_2CO in the spectral range of the C $1s$ and O $1s$ electron binding energies. The *ab initio* results for the (vertical electronic) energies and intensities are based essentially on a polarization propagator method [12,13] referred to as second-order algebraic diagrammatic construction [ADC(2)] used successfully in other studies of molecular *K*-shell excitation [8,9,14,15]. The vibrational excitations accompanying the electronic transitions and the vibronic coupling in the low-lying C $1s$ excited states $^1B_1(\pi^*)$, $^1B_2(2p\text{-}2h)$, $^1A_1(3s)$, and $^1A_2(3d)$ were studied using a model of vibronic coupling [16], whose parameters were derived from the ADC(2) results and from additional multireference configuration-interaction (MRCI) computations. In a similar fashion studies of *K*-shell excitation studies have been performed earlier for the first-row hydrides [8], ethylene [9], CO, and N_2 [15].

II. THEORETICAL APPROACH AND COMPUTATIONAL DETAILS

A. Calculation of the vertical core-electron excitation spectrum

The energies and intensities of the *K*-shell electron excitations have been computed using the second-order algebraic diagrammatic construction [ADC(2)] approximation scheme for polarization propagator [12–14]. The central computational step of this method is the eigenvalue problem

$$(\mathbf{K}+\mathbf{C})\mathbf{Y}=\mathbf{Y}\Omega, \quad \mathbf{Y}^\dagger\mathbf{Y}=1 \tag{1}$$

for the Hermitian secular matrix $\mathbf{K}+\mathbf{C}$ of the ''effective interaction,'' defined with respect to the configuration space of generalized (intermediate) single or particle-hole ($p\text{-}h$) and double or two-particle–two-hole ($2p\text{-}2h$) excitations. The resulting eigenvalues

$$\Omega_i=E_i-E_o \tag{2}$$

are the transition energies between the ground and the excited electronic states, characterized by the total energies E_o and E_i, respectively. The corresponding eigenvectors $\mathbf{Y}_i$ contain the information on the final states and allow for evaluation of the dipole transition moments according to the equation

$$T^\mu_{oi}=\mathbf{F}(\hat{D}_\mu)^\dagger\mathbf{Y}_i, \tag{3}$$

where $\mathbf{F}(\hat{D}_\mu)$ is the so-called vector of ''modified transition moments,'' depending on the dipole operator component $\hat{D}_\mu$. The photoabsorption intensities of the dipole-allowed transitions are given by the oscillator strengths

$$f_{oi}=\frac{2}{3}\Omega_i\sum_\mu |T^\mu_{oi}|^2, \tag{4}$$

where the summation runs over the three Cartesian components μ of the dipole transition moment. In the ADC(2) scheme the elements of the matrix $\mathbf{K}+\mathbf{C}$ and of the vector $\mathbf{F}(\hat{D}_\mu)$ are given by finite perturbation expansions through second order in the (residual) electronic interaction. The excitation energies and transition moments associated with singly excited states are treated consistently through second order of perturbation theory, while doubly excited states are treated consistently through first order.

Several important properties make the ADC(2) scheme especially attractive for the present study. First of all, the energies and transition moments are computed directly in a one-shot procedure circumventing a possible inconsistent description of the initial and final states. The ADC(2) computational procedure combines in an advantageous way variational and perturbative techniques, leading to a more compact configurational space than in a comparable configuration-interaction (CI) treatment. Another advantage relative to the CI approach is that the ADC(2) is a size-consistent method [17]. Finally, the ADC(2) scheme can easily be specialized to the case of *K*-shell excitation by adopting the core-valence separation (CVS) approximation [18,14]. In this approximation one neglects the interaction of the core- and the valence-shell excited states, which usually is weak due to the large core-valence energy gap and small coupling matrix elements. The CVS approximation leads to a considerable simplification of the ADC(2) equations [14] and to a further reduction of the configuration space, comprising now only configurations with one core hole. Thus, at the expense of a relatively small error (~0.5–1.0 eV according to estimates of Refs. [14,15]), the CVS approximation reduces substantially the computational expense of *K*-shell excitation calculations.

B. Framework for treating nuclear dynamics

To study the vibrational fine structure of the core-electron excitations we use the formalism of linear vibronic coupling (LVC) [16], capable of treating a variety of problems, including the general case of several electronic states interact-

ing via a set of nontotally symmetric vibrational modes. The approach is based on the concept of *diabatic* electronic states $|\Phi_i\rangle$ [19] which are used as a basis for expanding the final vibronic states

$$|\Psi_m(\mathbf{r},\mathbf{Q})\rangle = \sum_i |\chi_{im}(\mathbf{Q})\rangle |\Phi_i(\mathbf{r},\mathbf{Q})\rangle. \tag{5}$$

Here the summation runs over the *N*-dimensional set of vibronically coupled electronic states, and **r** and **Q** denote collectively the electronic and nuclear coordinates, respectively. The energy levels e_m and the expansion coefficients $|\chi_{im}\rangle$ (vibrational wave functions) are determined from the eigenvalue equation

$$\hat{\mathbf{H}}\chi_m = e_m\chi_m \tag{6}$$

for the $N\times N$ matrix LVC model Hamiltonian $\hat{\mathbf{H}}$ whose elements are given by Taylor expansions of the potential-energy functions through linear terms in the nuclear coordinates:

$$(\hat{\mathbf{H}})_{ij} = \begin{cases} \hat{H}_o + \Omega_i + \sqrt{2}\sum_{s\in g} \kappa_i^s Q_s, & i=j \\ \sqrt{2}\sum_{s\in u} \lambda_{ij}^s Q_s, & i\neq j. \end{cases} \tag{7}$$

Here Ω_i denote vertical electronic transition energies associated with the states $|\Phi_i\rangle$, κ_i^s and λ_{ij}^s are the *intrastate* and *interstate* coupling constants, respectively, and Q_s are the displacements of the totally symmetric (*g*) or nontotally symmetric (*u*) normal modes ν_s. The vibrational Hamiltonian

$$\hat{H}_o = \frac{1}{2}\sum_{s\in g,u} \omega_s \left(-\frac{\partial^2}{\partial Q_s^2} + Q_s^2 - 1 \right) \tag{8}$$

refers to the electronic ground state $|\Phi_o\rangle$ and describes noninteracting harmonic oscillators with frequencies ω_s. In Eq. (8) the vibrational ground-state energy has been chosen as the origin of the energy scale. As a characteristic feature of the diabatic formulation, $\hat{\mathbf{H}}$ introduces the coupling between the electronic states via the potential energy rather than via the kinetic energy of the nuclei.

For the solution of Eq. (6) a variational ansatz is employed, assuming an expansion of the vibrational wave function $|\chi_{im}\rangle$ in a direct-product basis $|n_1\cdots n_M\rangle$ of harmonic-oscillator eigenstates of $\hat{H}_o$,

$$|\chi_{im}\rangle = \sum_{n_1\cdots n_M} C_{im}^{n_1\cdots n_M} |n_1\cdots n_M\rangle. \tag{9}$$

Here the summation is performed over all possible combinations of quantum numbers associated with the individual modes (*M* is the total number of modes in both sets *g* and *u*). In actual calculations, of course, one restricts the expansion [Eq. (9)] by specifying a maximal level of excitation (in terms of quantum numbers n_s) for each of the modes ν_s.

Once the final energies levels e_m and the corresponding wave functions $|\chi_{im}\rangle$ have been determined, the spectral function describing the excitation from the zero vibrational level $|\chi_{00}\rangle$ of the electronic ground state $|\Phi_0\rangle$ into the manifold of vibronically interacting states $|\Phi_i\rangle$ can be evaluated according to the expression

$$P(E) = \sum_m f_{oi(m)} |\langle \chi_{00}|\chi_{im}\rangle|^2 \delta(E - e_m), \tag{10}$$

where $f_{oi(m)}$ indicates the oscillator strength for the single electronic state contributing to a given vibronic final state *m*. Note that Eq. (10) applies only to the case where the considered electronic states belong to different symmetry species. In the case of noninteracting states [that is when all λ_{ij}^s in Eq. (7) vanish] Eq. (10) reduces to a superposition of vibrational progressions [16,20]

$$P(E) = \sum_i f_{oi} \sum_{n_1\ldots,n_g} |\langle 0...0|n_1\ldots n_g\rangle|^2 \times \delta\left(E - \Omega_i + \sum_{s\in g} \omega_s(a_{is} - n_s) \right). \tag{11}$$

Here each progression represents a spectrum for a shifted harmonic oscillator (described by a Poisson intensity distribution), the Franck-Condon factors being given by

$$|\langle 0\ldots 0|n_1\ldots n_g\rangle|^2 = \prod_{s\in g} \frac{(a_{is})^{n_s}}{n_s!} e^{-a_{is}}, \tag{12}$$

where $a_{is} = (\kappa_i^s/\omega_s)^2$ is the so-called Poisson (or vibrational strength) parameter. The spectral intensities according to Eq. (10) can efficiently be evaluated without explicit exact diagonalization of Hamiltonian matrix by using the Lanczos algorithm [21,16], which allows one to obtain quite accurate spectral envelopes at moderate computational cost.

For the LVC calculations, one has to determine the model parameters Ω_i, f_{oi}, ω_s, κ_i^s, and λ_{ij}^s for the problem under consideration. While the values of Ω_i and f_{oi} can readily be taken from ADC(2) or CI calculations, and ω_s can be approximated by the ground-state vibrational frequencies computed within one of the standard *ab initio* schemes, the determination of coupling constants κ_i^s and λ_{ij}^s is less standard. The intrastate coupling constants κ_i^s associated with the totally symmetric modes can be obtained with the aid of the relation [16]

$$\kappa_i^s = \frac{1}{\sqrt{2}} \left(\frac{\partial \Omega_i(\mathbf{Q})}{\partial Q_s} \right)_{\mathbf{Q}_0}, \quad s\in g \tag{13}$$

where $\Omega_i(\mathbf{Q})$ denotes the energy of the *i*th electronic transition at the nuclear configuration **Q**. In the present work the derivatives were evaluated numerically. For this purpose the excitation energies were computed at the nuclear configurations $\mathbf{Q}_s' = \mathbf{Q}_0 \pm \Delta_s$ obtained by taking the step $\pm\Delta_s$ from $\mathbf{Q}_0$ along the dimensionless normal coordinate Q_s [22]. The latter quantities were derived from the Cartesian normal modes

TABLE I. Ground-state bond lengths, angles, and vibrational frequencies of H_2CO.

Parameter		MP2[a]	CCSD[b]	Expt.[c]
Geometry				
R_{CO} (Å)		1.2126	1.2049	1.2072
R_{CH} (Å)		1.0995	1.1005	1.1171
∠H—C—H		116.64°	116.57°	116.23°
Vibrational frequencies (cm^{-1})				
$\nu_1(a_1)$	Symmetric CH stretching	2973	2955	2783
$\nu_2(a_1)$	CO stretching	1751	1808	1746
$\nu_3(a_1)$	CH_2 bending	1550	1557	1500
$\nu_4(b_1)$	out-of-plane bending	1188	1194	1167
$\nu_5(b_2)$	antisymmetric CH stretching	3050	3026	2843
$\nu_6(b_2)$	CH_2 rocking	1281	1289	1249

[a]Total energy (basis A): $E_{HF}=-113.906\,559$ a.u., $E_{MP2}=-114.280\,221$ a.u.
[b]Total energy (basis B): $E_{HF}=-113.906\,108$ a.u., $E_{CCSD}=-114.286\,945$ a.u.
[c]Reference [27], as cited in Ref. [2].

computed together with ω_s. The interstate coupling constants λ_{ij}^s can be obtained in a similar way using the relation [16]

$$\lambda_{ij}^s=\frac{1}{2\Delta_s}([\Omega_i(\mathbf{Q}_s')-\Omega_j(\mathbf{\Omega}_s')]^2-[\Omega_i^0-\Omega_j^0]^2)^{1/2},\quad s\in u \tag{14}$$

where $\Omega_m^0=\Omega_m(\mathbf{Q}_0)$. Alternatively, the constants λ_{ij}^s can be determined by fitting the Q_s dependence of the adiabatic excitation energy of the lower (ith) state derived from the LVC model,

$$\Omega_i(\Omega_s)=\tfrac{1}{2}\{\Omega_i^0+\Omega_j^0-([\Omega_i^0-\Omega_j^0]^2+8(\lambda_{ij}^s)^2Q_s^2)^{1/2}\},\quad s\in u \tag{15}$$

to the results of the *ab initio* calculations. Here the vertical excitation energy Ω_j^0 of the upper (jth) state may be treated as another variational parameter. We note that the above expressions can easily be adapted to total CI energies $U_i(\mathbf{Q})$, since $\mathbf{\Omega}_i(\mathbf{Q})=U_i(\mathbf{Q})-U_0(\mathbf{Q})$.

C. Basis sets

Three basis sets were used in the present study. The basis *A* was constructed from the uncontracted $(9s5p)$ and $(4s)$ Gaussian basis sets of Huzinaga [23] (a scaled form of the hydrogen basis fitting the Slater exponent $\zeta=1.2$ was adopted), by adding polarization functions from the corresponding *cc-pVTZ* (correlation consistent–polarized valence double zeta) sets of Dunning [24] (no *f* functions or H-centered *d* functions were included) and diffuse functions on C ($\zeta_s=0.02$, $\zeta_p=0.04$, $\zeta_d=0.06$) and on O ($\zeta_s=0.04$, $\zeta_p=0.06$, $\zeta_d=0.08$). The six-component Cartesian representation of *d* functions has been used. The total number of molecular orbitals (MO) in basis *A* is 112. The same basis using, however, the five-component spherical representation of *d* functions is referred to as basis *B* (106 MO). Finally, basis *C* (132 MO) was obtained from basis *A* by adding the diffuse functions $\zeta_s=0.003\,35$, $0.002\,05$; $\zeta_p=0.005\,69$, $0.003\,48$; $\zeta_d=0.008\,08$, $0.004\,93$ [25] at the molecular center of mass.

D. Ground-state parameters

The equilibrium ground-state geometry and the corresponding vibrational frequencies ω_s of H_2CO were computed using the second-order Møller-Plesset perturbation theory (MP2) with the basis *A*, as well as using the coupled-cluster singles and doubles (CCSD) method with basis *B*. These calculations were performed with the GAUSSIAN program package [26]. The results are shown in Table I together with the experimental data [27], as cited in Ref. [2]. The MP2 and CCSD geometries are quite similar, showing marginal improvements at the CCSD level. Both sets of results agree well with the experimental data. The vibrational frequencies are reproduced also very satisfactorily by the calculations, the MP2 results being somewhat closer to the experimental data. The MOLDEN software [28] was used for visualization of the ground-state Hartree-Fock (HF) molecular orbitals (Sec. III B).

E. The ADC(2) and MRCI calculations

The ADC(2)/CVS calculations were performed using basis *C* which, according to our previous experience [8,15], should be adequate to describe at least the first two members the of *s*, *p*, and *d* Rydberg series. The original ADC(2) code [13] interfaced to the GAMESS program package [29] was used throughout. In the C $1s$ calculations the O $1s$ MO was kept frozen and vice versa.

Additional MRCI calculations were performed for the three lowest C $1s$ excited states $^1B_1(\pi^*)$, $^1B_2(2p\text{-}2h)$, and $^1A_1(3s)$. Here basis *B* was used. The MRCI expansions were based on relaxed MO's generated by a HF calculation for the C $1s^{-1}$ cationic state; they included all C $1s$ hole configuration state functions (CSF) constructed as single and double excitations with respect to a given reference set. The reference set included all CSF's with absolute value of the expansion coefficient $\geqslant 0.04$ and its weight in the final MRCI

TABLE II. Adiabatic $\Omega_{0\text{-}0}$ and vertical Ω_v excitation energies (eV), absolute oscillator strengths (f), and intrastate vibronic coupling constants k_s (eV) for singlet C $1s$ transitions of H_2CO. Vertical triplet ($S=1$) excitation energies are given in the last column.

Transition C $1s\rightarrow$	Expt.[a]	This work, ADC(2)						
	$\Omega_{0\text{-}0}$	$\Omega_{0\text{-}0}$	Ω_v	f	k_1	k_2	k_3	$\Omega_v\,(S=1)$
$\pi^*\,(B_1)$	285.59	285.18	285.64	0.0563	0.306	−0.204	0.050	284.69
$2p\text{-}2h\,(B_2)$		290.09	292.06	1×10^{-5}	0.352	−0.569	0.165	292.06
$3s\text{-}a_1$	290.18	290.19	290.23	0.0064	0.055	0.040	−0.071	289.71
$3p\text{-}b_2$	291.25	291.17	291.25	0.0176	0.100	0.021	−0.100	290.86
$3p\text{-}a_1$		291.21	291.30	0.0001	0.180	0.030	−0.011	291.29
$3p\text{-}b_1$	291.73	291.56	291.71	0.0074	0.190	0.045	−0.087	291.55
$4s\text{-}a_1$	292.22	292.14	292.32	0.0021	0.051	−0.021	−0.182	292.19
$3d\text{-}a_1$		292.57	292.71	<0.0001	0.187	0.036	−0.088	292.72
$3\tilde{d}\text{-}a_1$		292.61	292.74	0.0001	0.183	0.040	−0.073	292.74
$3d\text{-}a_2$		292.63	292.77		0.181	0.034	−0.097	292.77
$3d\text{-}b_2$	292.76	292.69	292.79	0.0041	0.158	0.025	−0.073	292.69
$3d\text{-}b_1$		292.74	292.88	<0.0001	0.186	0.036	−0.086	292.88
$4p\text{-}b_2$	292.98	292.77	292.90	0.0020	0.173	0.037	−0.094	292.88
$4p\text{-}a_1$		292.80	292.93	0.0001	0.185	0.030	−0.077	292.92
$4p\text{-}b_1$	293.09	292.87	293.01	0.0026	0.185	0.039	−0.087	292.95
$5s\text{-}a_1$		293.04	293.18	0.0007	0.136	0.012	−0.128	293.15
$4d\text{-}a_1$		293.23	293.37	<0.0001	0.187	0.036	−0.088	293.37
$4d\text{-}a_2$		293.26	293.40		0.182	0.034	−0.093	293.40
$4\tilde{d}\text{-}a_1$		293.27	293.40	<0.0001	0.183	0.037	−0.080	293.39
$4d\text{-}b_2$	293.56	293.30	293.41	0.0022	0.167	0.035	−0.077	293.37
$4d\text{-}b_1$		293.33	293.47	0.0001	0.185	0.035	−0.086	293.47
$5p\text{-}b_2$		293.35	293.49	0.0012	0.177	0.037	−0.093	293.48
$5p\text{-}a_1$		293.38	293.51	0.0001	0.184	0.032	−0.080	293.50
$5p\text{-}b_1$	293.46	293.42	293.56	0.0022	0.185	0.040	−0.088	293.52

[a]Reference [2].

wave functions was about 0.9. The multireference Davidson correction was included to account for the effect of unlinked terms in the CI expansion. The O $1s$ orbital and the four highest virtual MO's were frozen in these calculations. For the MRCI calculations the direct CI [30] program of the GAMESS-UK package [31] was used.

III. ELECTRONIC TRANSITIONS AND VIBRATIONAL EXCITATION

A. Core-to-valence transitions

The $\tilde{X}\ ^1A_1$ ground-state electronic configuration of formaldehyde is

$$1a_1(\mathrm{O}\ 1s)^2 2a_1(\mathrm{C}\ 1s)^2 3a_1^2 4a_1^2 1b_2^2 5a_1^2 1b_1(\pi)^2 2b_2(n)^2 \cdots b_1(\pi^*)^0,$$

where the highest occupied MO's $2b_2$ and $1b_1$ correspond to the oxygen lone-pair (n) and to the π orbital, respectively. The unoccupied antibonding $\pi^*(b_1)$ orbital becomes populated in the transitions C $1s\rightarrow\pi^*(^1B_1)$ and O $1s\rightarrow\pi^*(^1B_1)$ leading to the most prominent features (also referred to as π^* resonances) in the *K*-shell absorption spectra. The excitation of C $1s$ and O $1s$ electrons to higher unoccupied MO's give rise to series of Rydberg transitions converging to the respective ionization limits.

In Tables II and III the results of our calculation for the vertical and adiabatic *K*-shell transitions of H_2CO are shown together with the experimental data of Remmers *et al.* [2]. Here the adiabatic transition energies correspond to 0-0 transitions. At this stage the Poisson intensity distribution (PID) model [Eq. (11)] was used to simulate the vibrational structure of the electronic bands. The coupling parameters κ_i^s (also shown in Tables II and III) were calculated according to Eq. (13) using ADC(2) vertical excitation energies and the ground-state normal coordinates at the MP2 level. Also the vibrational frequencies ω_s were taken from the MP2 treat-

TABLE III. Adiabatic $\Omega_{0\text{-}0}$ and vertical Ω_v excitation energies (eV), absolute oscillator strengths (f), and intrastate vibronic coupling constants k_s (eV) for singlet O 1s transitions of H_2CO. Vertical triplet ($S=1$) excitation energies are given in the last column.

Transition O 1$s\rightarrow$	Expt.[a]	This work, ADC(2)						
	$\Omega_{0\text{-}0}$	$\Omega_{0\text{-}0}$	Ω_v	$10f$	k_1	k_2	k_3	Ω_v ($S=1$)
π^* (B_1)	530.82	528.95	529.54	0.4132	0.106	−0.344	0.054	528.99
3s-a_1	535.43	533.81	533.96	0.0054	0.023	−0.168	−0.060	533.93
3p-a_1	536.34	534.62	534.74	0.0079	0.025	−0.155	0.036	534.52
3p-b_2		534.78	534.94	<0.0001	0.036	−0.165	−0.074	534.95
3p-b_1		535.03	535.15	0.0009	0.065	−0.146	−0.054	535.16
4s-a_1		535.62	535.86	0.0003	0.002	−0.194	−0.113	535.86
3d-a_1		535.88	535.99	0.0078	0.044	−0.148	−0.040	535.96
3d-a_2		535.98	536.12		0.062	−0.157	−0.058	536.12
3$\tilde{d}$-a_1		535.99	536.12	0.0052	0.064	−0.154	−0.046	536.11
3d-b_2	537.78	536.03	536.16	0.0122	0.052	−0.153	−0.047	536.13
3d-b_1		536.07	536.20	0.0060	0.064	−0.151	−0.049	536.19
4p-a_1		536.15	536.28	0.0011	0.059	−0.158	−0.035	536.23
4p-b_2		536.18	536.32	0.0001	0.054	−0.156	−0.058	536.32
4p-b_1		536.25	536.38	0.0005	0.064	−0.150	−0.052	536.39
5s-a_1		536.41	536.60	<0.0001	0.028	−0.179	−0.088	536.60
4d-a_1		536.55	536.68	0.0040	0.061	−0.151	−0.045	536.66
4d-a_2		536.60	536.74		0.062	−0.156	−0.055	536.74
4$\tilde{d}$-a_1		536.62	536.75	0.0033	0.064	−0.154	−0.047	536.75
4d-b_2	538.46	536.64	536.77	0.0083	0.055	−0.154	−0.047	536.76
4d-b_1		536.67	536.80	0.0040	0.064	−0.153	−0.050	536.80
5p-a_1		536.72	536.85	0.0006	0.060	−0.157	−0.042	536.83
5p-b_2		536.74	536.88	0.0005	0.057	−0.154	−0.058	536.88
5p-b_1		536.80	536.93	0.0010	0.064	−0.148	−0.054	536.94

[a]Reference [2].

ment (Table I). In Figs. 1 and 2 the resulting theoretical photoabsorption profiles are shown together with the experimental spectra [2]. The theoretical spectral envelopes were obtained by convoluting the spectral functions [Eq. (11)] with Lorentzians of 0.14 and 0.20 eV full width at half maximum (FWHM), respectively, in order to reproduce the average natural linewidth of the C 1s and O 1s excitations.

Concerning the absolute accuracy of our results, we note that a relativistic correction of 0.1 and 0.4 eV has to be added to the calculated excitation energies [32]. This improves the agreement between theory and experiment: in the C 1s and O 1s case the mean deviation reduces to 0.04 and 1.36 eV, respectively, while the maximal deviation is 0.31 and 1.47 eV, respectively. As discussed in Refs. [14,15,3], the larger discrepancies in the O 1s case reflect the larger relaxation energy of the O 1s core hole states, not fully accounted for by the present second-order treatment. The relaxation energy error of our K-shell calculations leads essentially to a uniform shift of the excitation energies, being characteristic to the respective core hole [15]. This means that irrespective of the absolute accuracy the relative ADC(2) energies give a good description of the experimental data. Accordingly, the theoretical spectra in Figs. 1 and 2 have been aligned to the experimental spectra. The comparison of the present results with the ADC(2) calculations of Ref. [3] shows discrepancies

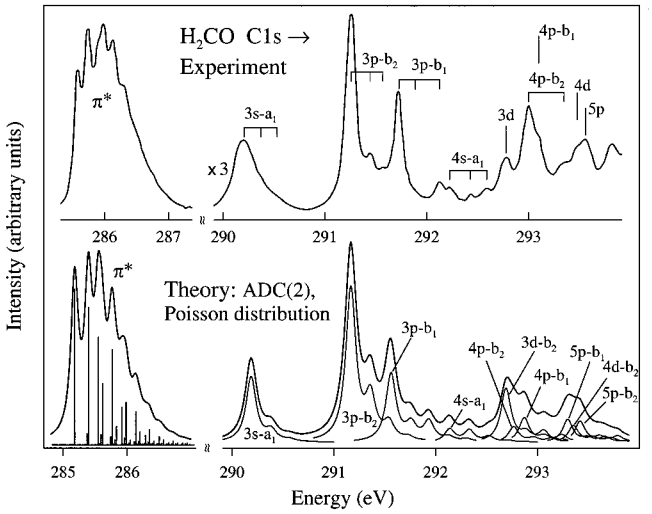

FIG. 1. Theoretical and experimental [2] C 1s photoabsorption spectra of H_2CO. The experimental C 1s Rydberg spectrum (above 290 eV) has been magnified by a factor close to 3. The lower panel shows in addition to the total theoretical spectrum also the contributions of the individual electronic transitions. The theoretical curves have been generated by convoluting the bar spectra with Lorentzians of 0.14 eV (total curve) and 0.12 eV (individual contribution) FWHM, respectively.

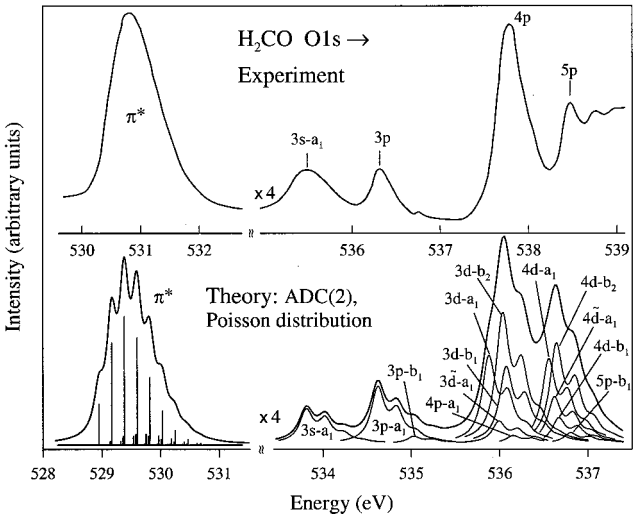

FIG. 2. Theoretical and experimental [2] O 1*s* photoabsorption spectra of H_2CO. The experimental and theoretical O 1*s* Rydberg spectra (above 533 eV) have been magnified by a factor close to 4. The lower panel shows in addition to the total theoretical spectrum also the contributions of the individual electronic transitions. The theoretical curves have been generated by convoluting the bar spectra with Lorentzians of 0.20 eV (total curve) and 0.18 eV (individual contribution) FWHM, respectively.

of 0.4 and 0.5 eV for the C 1*s* and O 1*s* excitations, respectively. Apart from basis-set differences the previous results were affected by a bug in the old computer code concerning the diagonal secular matrix elements of certain double excitations. A better agreement is found for the oscillator strengths. The present *f* values 0.0563 and 0.0413 for the C 1*s* and O $1s\rightarrow\pi^*$ resonances, respectively, differ only slightly from the *f* values 0.0551 and 0.0402 of Ref. [3]. The theoretical C 1*s* photoabsorption profile in Fig. 1 reproduces qualitatively correctly all major features due to electronic and vibrational transitions of the experimental C 1*s* spectrum [2]. Here, not only the relative positions, but also the intensities of the peaks are seen to be in a good qualitative agreement with the measurements. The prominent C $1s\rightarrow\pi^*$ band centered at about 286 eV of the C 1*s* spectrum [2] is formed mainly by the excitation of the ν_1 and ν_2 modes, for which large coupling constants κ_i^s have been found. This supports the conclusions of Remmers *et al.* [2] about the importance of these two modes for the C $1s\rightarrow\pi^*(^1B_1)$ transition. A more detailed discussion of the fine structure of the π^*-resonance band based on the results of our vibronic coupling calculations is given in Sec. IV.

In contrast to the π^* excitation in the C 1*s* spectrum, the O $1s\rightarrow\pi^*(^1B_1)$ transition does not show resolved vibrational structure. This is somewhat puzzling as our PID results here predict a well-structured spectral envelope. With the experimental resolution of 0.15 eV achieved in Ref. [2] this structure should be observable in the spectrum and its absence is consequently due to effects not accounted for by the present model. One possible cause is a strong reduction of the final-state vibrational frequencies with respect to those of the ground and the C 1*s* excited states, as was observed in the similar case of CO [6,15]. Alternatively, a dissociation process may take place after vertical excitation to the $^1B_1(\mathrm{O}\,1s\rightarrow\pi^*)$ state. Also the excitation of many nontotally symmetric modes as a result of vibronic interaction with higher excited states would obliterate resolvable structure, a possibility that cannot be excluded.

TABLE IV. Origination of the lowest Rydberg series in core-excited H_2CO: splitting of atomic *s*, *p*, and *d* orbitals in the molecular field.

Atom	Molecule (C_{2v} point group)			
	A_1	B_1	B_2	A_2
s	$ns\text{-}a_1$			
p	$np\text{-}a_1$	$np\text{-}b_1$	$np\text{-}b_2$	
d	$nd\text{-}a_1$, $n\tilde{d}\text{-}a_1$	$nd\text{-}b_1$	$nd\text{-}b_2$	$nd\text{-}a_2$

In spite of its low dipole oscillator strength (1×10^{-5}), a truly remarkable feature in the C 1*s* spectrum of H_2CO is the presence of the low-lying double excitation C $1s,n\rightarrow\pi^{*2}(^1B_2)$, which according to the MRCI estimates of Ref. [3] should be expected at 288.9 eV. In the ADC(2) treatment the energy of this transition is grossly overestimated (292.06 eV) due to the inherently poorer description of the double excitations, and one has to refer to the more accurate MRCI result (288.5 eV, according to the present calculations) here. The C $1s,n\rightarrow\pi^{*2}$ transition will be discussed further in Sec. IV in the context of our vibronic coupling study of the low-energy part of the C 1*s* excitation spectrum.

B. Core-to-Rydberg transitions

The Rydberg states are typically viewed as hydrogenic *nl* states split by the molecular field, which in the case of H_2CO ($C_{2\nu}$ point group) gives rise to the manifold of $nl\gamma$ states listed in Table IV (here the index γ denotes the irreducible representation of the orbital). The vertical excitation energies $\Omega_{nl\gamma}$ are usually well described by a Rydberg formula

$$\Omega_{nl\gamma}=I-R(n-\delta_{l\gamma})^{-2}, \tag{16}$$

where *I* denotes the vertical ionization energy, *R* is the Rydberg constant, *n* is the principal quantum number, and $\delta_{l\gamma}$ is the quantum defect of the $l\gamma$ series. Equation (16) normally holds to a good approximation for all members of the same $l\gamma$ series and thus can be used for the verification of assignments. In Table V we present the results of an optimization procedure by which Eq. (16) was fitted to the vertical ADC(2) excitation energies based on the assignments of Tables II and III. The fitted C 1*s* and O 1*s* ionization energies (common for all Rydberg series) are 294.22 and 537.57 eV, respectively, which should be compared to the experimental values 294.35 and 539.30 eV [2]. The observed differences of 0.13 and 1.73 eV are consistent with the average differences between the present adiabatic excitation energies and the experimental data of Remmers *et al.* [2] (0.14 and 1.76 eV, respectively). The resulting quantum defects are within their typical experimental limits ($1.1\leqslant\delta_s\leqslant1.2$, $0.6\leqslant\delta_p\leqslant0.9$, $-0.2\leqslant\delta_d\leqslant0.1$). The accuracy of the present fit

TABLE V. Quantum defects of various Rydberg series of core-excited H_2CO obtained by fitting the Rydberg formula to the ADC(2) vertical excitation energies

Series	C 1s[a]	O 1s[b]
ns-a_1	1.17	1.07
np-a_1	0.83	0.80
np-b_1	0.67	0.62
np-b_2	0.85	0.72
nd-a_1	0.0	0.07
nd-b_1	−0.19	−0.16
nd-b_2	−0.08	−0.08
$n\tilde{d}$-a_1	−0.03	−0.06
nd-a_2	−0.06	−0.05

[a]Fitted ionization energy: $I=294.22$ eV.
[b]Fitted ionization energy: $I=537.57$ eV.

(with mean square deviations of 0.06 and 0.04 eV for the C 1s and O 1s excitations, respectively) could not be improved by using other trials for arranging the ADC(2) results into Rydberg series (e.g., by interchanging the nd and $(n+1)p$ members of a series within the same symmetry species γ).

The maximal splitting Δ_{nl} of the nl manifolds decreases for higher n ($\Delta_{np}=0.46$, 0.11, and 0.07 eV for $n=3$, 4, and 5 and $\Delta_{nd}=0.17$ and 0.10 eV for $n=3$ and 4). Along with this trend, the intensity of the dipole-allowed transitions drops as n increases. In most cases the triplet states lie somewhat below the corresponding singlet states or they even coincide with the singlets. The present calculations should describe the K-shell Rydberg excitations in H_2CO reliably up to (at least) $n=4$. This is a distinct improvement over the previous ADC(2) results of Ref. [3] suffering from the lack of diffuse d functions in the AO basis. The same deficiency affects the theoretical studies reported in Refs. [4,5], although in principle the methods used should obtain a better absolute accuracy than the present ADC(2) approach.

1. C 1s excitation spectrum

As seen in Fig. 1 the largest contribution to the C 1s Rydberg spectrum arises from members of the ns-a_1, ns-b_2, np-b_1, and nd-b_2 Rydberg series. This is consistent with the assignment of Remmers *et al.* [2], who could not specify, however, the actual symmetry of the dominant nd excitations. In agreement with previous assignments [1–5], we find that the prominent features at 290.18, 291.25, and 291.73 eV correspond to the 0-0 lines of the $3s$-a_1, $3p$-b_2, and $3p$-b_1 Rydberg transitions, respectively. The structure accompanying these bands at the high-energy side is due to vibrational excitation: The poorly resolved high-energy shoulders of the $3s$-a_1 band can be interpreted as the 3_0^1 and 1_0^1 excitations, while the maxima seen just after the $3p$-b_2 and $3p$-b_1 peaks can be identified as the 3_0^1 vibrational sidebands.

The assignment of the smaller spectral features is more difficult because of the presence of weaker dipole-allowed transitions not shown in Fig. 1, but listed in Table II. The 0-0 lines of such transitions compete in intensity with the vibrational sidebands of the stronger transitions located nearby. An example is the $3p$-a_1 transition, which may contribute to a small maximum at 291.4 eV and to a shoulder at 291.6 eV between the $3p$-b_2 and $3p$-b_1 peaks in the spectrum [2]. Alternatively, as seen from the theoretical spectral profile, these features can as well be interpreted as a vibrational structure of the $3p$-b_2 transition. At higher energy we can confirm only the assignment of the well-separated structure around 292.22 eV [2] as being due to the $4s$-a_1 transition. According to our results the features at 292.76 and 292.98 eV are composite structures arising from vibrational progressions of several $3d$ and $4p$ transitions. In a similar way, the feature at 293.5 eV [2] combines contributions from various $4d$ and $5p$ transitions.

As can be seen from the intrastate coupling constants and the vibrational frequencies, the vibrational excitation patterns of most C 1s Rydberg transitions are quite similar. The ν_1 and ν_2 modes (symmetric CH and CO stretching, respectively) are predicted to be the most active ones, while the ν_3 mode (H—C—H symmetric bending) is expected to be only weakly excited.

2. O 1s excitation spectrum

The O 1s photoabsorption spectrum (Fig. 2) differs markedly from the C 1s spectrum [1,2]. Besides the increased linewidth and the lack of resolved vibrational structure one finds in comparison to the C 1s case an extensive redistribution of intensity between the spectral features. The latter effect is most pronounced for the three lowest Rydberg bands at 535.43, 536.34, and 537.78 eV, assigned in Ref. [2] to the $3s$, $3p$, and $4p$ transitions, respectively. While in the C 1s spectrum the $3p$ transitions are clearly dominating, their total intensity in the O 1s case drops to that of the $3s$ peak. The peak attributed to the $4p$ transition, on the other hand, is seemingly the strongest feature in the O 1s Rydberg manifold. The apparent increase of intensity contradicts the usual n^{-3} behavior of np Rydberg intensities, and, thus, one may suspect that besides the $4p$ transition other important contributions must be present in the 537.78 eV peak of the O 1s spectrum [2]. According to our ADC(2) results this is indeed the case: the main intensity contributions in this energy region arise from dipole-allowed $3d$ Rydberg transitions ($3d$-a_1, $3\tilde{d}$-a_1, $3d$-b_1, and $3d$-b_2). As can be seen in Table III, the oscillator strengths of these transitions are much larger than those of the $4p$-a_1, $4p$-b_1, and $4p$-b_2 transitions. For the next higher peak in the O 1s spectrum we find the same situation for the $5p$ and $4d$ transitions. The comparison of the absolute oscillator strengths in Tables II and III shows that the intensity of the $3d$ transitions in the O 1s spectrum is of the same order of magnitude as in the C 1s spectrum, but the intensity of the np-b_2 and np-b_1 series is substantially smaller. The suppression of the np transitions increases the relative importance of the other O 1s transitions, so that the spectral O 1s profile differs profoundly from the C 1s spectrum. A similar effect can be observed in the np-π Rydberg transitions in the O 1s photoabsorption spectrum of CO [6,15].

To a certain extent the differences between the C 1s and O 1s transition strengths reflect the localization properties of

the unoccupied (virtual) orbitals. For example, the π^* orbital is biased towards the carbon site and accordingly the magnitude of the C $1s\rightarrow\pi^*$ dipole transition moment should be larger than that of the O $1s\rightarrow\pi^*$ transition. This is indeed confirmed by our calculations yielding absolute f values of 0.0563 and 0.0413 for the C $1s\rightarrow\pi^*$ and O $1s\rightarrow\pi^*$ transition, respectively. Apparently, localization features are found as well for certain low-lying Rydberg states in H_2CO (and CO [15]). According to an analysis of the final-state wave functions the *np* Rydberg states are predominantly localized on the CH bond. The *nd* orbitals, on the other hand, show a more typical Rydberg orbital behavior, that is, they are more uniformly spread over the entire molecule. This explains why the intensity of O $1s-np$ transitions is smaller than that of the O $1s-nd$ transitions. The origin of the ''partial localization'' of the *np*-type orbitals in H_2CO (and CO) is not fully established. In principle, localization of Rydberg orbitals can be ''modulated'' by admixtures of valence π^* or σ^* character. In particular, σ^* character seems to be present in the np-b_2 orbitals, leading to a bias towards the CH bonds. By contrast to the situation for the *np* orbitals, the hydrogenic character of the *nd* Rydberg orbitals is not affected by valence orbital admixtures.

The first Rydberg transition in the experimental O $1s$ spectrum [2] at 535.43 eV can unambiguously be assigned to the $3s$-a_1 excitation [1–5]. According to our results the next spectral maximum at 536.34 eV [2], generically designated by Remmers *et al.* [2] as ''$3p$,'' originates mainly from the $3p$-a_1 transition, while in contrast to the C $1s$ spectrum the $3p$-b_1 and $3p$-b_2 transitions do not play a notable role here. The complex structure at 537.78 eV [2] is due to various dipole allowed $3d$ transitions, whereas the $4p$ contributions are not negligible but rather weak. Thus the assignment ''$4p$'' given to this feature by Remmers *et al.* [2] is not correct and should be replaced by ''$3d$'' or by ''$3d \gg 4p$.'' In addition, there are small $4s$-a_1 and $5s$-a_1 contributions here. In a similar way, the assignment of the next higher peak at 538.46 eV [2] should be changed from ''$5p$'' [2] to ''$4d$'' or to ''$4d \gg 5p$.''

Although the vibrational fine structure could not be resolved in the experiment, it is interesting to note that the vibrational excitation pattern predicted for the O $1s$ Rydberg states differs distinctly from that of the C $1s$ case. Here the ν_2 (CO bond stretching) is expected to be the most active one, while the modes ν_1 and ν_3 should be less excited.

C. Conformation changes in the C 1*s* and O 1*s* excited states

The coupling constants κ_i^s for the totally symmetric modes, shown in Tables II and III, allow for a qualitative survey of the excited state conformations. According to Eq. (13), a positive (negative) κ_i^s value indicates a decrease (increase) of the corresponding bond length or angle (with respect to the ground state). For the C $1s$ (and O $1s$) excited $^1B_1(\pi^*)$ state there is a distinct increase of the CO bond length ($\kappa_2<0$), reflecting the effect of populating the antibonding π^* orbital. Both the CH bond length and the H—C—H angle decrease as the corresponding coupling constants κ_1 and κ_3, respectively, are positive. This confirms the results of Remmers *et al.* [2], but disagrees with our previous ROHF (restricted Hartree-Fock) calculations [11] in the case of the H—C—H angle. Similar changes of the nuclear conformation are predicted for the C $1s,n\rightarrow\pi^{*2}(^1B_2)$ transition, here being fully consistent with our ROHF results [11].

As mentioned before, the $1s$ Rydberg excitations show essentially the same conformation changes as the ionic $1s$ hole states. For the C $1s$ case, we find a decrease of the CH and CO bonds ($\kappa_1>0$ and $\kappa_2>0$), while the H—C—H angle increases ($\kappa_3<0$). This is consistent with the predictions of our ROHF calculations for the $^1A_1(\mathrm{C}\,1s\rightarrow 3s\text{-}a_1)$ state [11] and also confirms the guess of Remmers *et al.* [2]. For O $1s$ ionization (and Rydberg excitation) the CO bond length increases ($\kappa_2<0$), whereas the CH bond length and the H—C—H angle behave as in the case of C $1s$ ionization.

The decrease ($\kappa<0$) or increase ($\kappa>0$) of the $1s$ ionization energy as the function of a bond length can be understood essentially as being the result of an electrostatic screening or antiscreening effect caused by the respective bond-length alternation. For example, the stretching of the CH bond removes charge from the C atom (antiscreening), leading thus to an increase of the C $1s$ ionization energy. Concerning the CO bond length, we find antiscreening for the C atom and screening for the O atom upon elongation. This can be understood by recalling that in the H_2CO ground state there is a correlation-induced charge transfer from oxygen to carbon (via partial population of the carbon-centered π^* orbital and depopulation of the oxygen-centered π orbital). As the CO bond increases, oxygen takes electronic charge back from carbon thus causing the observed screening and antiscreening effects for the O $1s$ and C $1s$ ionization, respectively.

IV. VIBRONIC COUPLING EFFECTS IN THE LOWEST C 1*s* EXCITATIONS

The important role of vibronic coupling effects for the lowest C $1s$ excited states $^1B_1(\pi^*)$, $^1B_2(2p\text{-}2h)$, and $^1A_1(3s)$ of H_2CO is indicated by the presence of double wells in the $^1B_1(\pi^*)$ and $^1B_2(2p\text{-}2h)$ potential-energy surfaces with respect to the out-of-plane bending coordinate ν_4 [11]. While H_2CO is predicted to be distinctly nonplanar in the $^1B_2(2p\text{-}2h)$ state (the out-of-plane angle is 59.7°, the stabilization energy is 0.344 eV), the $^1B_1(\pi^*)$ state can be characterized as being only quasiplanar, as the stabilization energy amounts only to 0.006 eV (at the MRCI level), so that the lowest vibrational level lies above the inversion barrier. The minimum of the $^1B_1(\pi^*)$ PES corresponds to an out-of-plane angle of 22.8° [11].

The vibronic coupling model considered in the following comprises the four lowest electronic states. The possible coupling modes are restricted by obvious symmetry selection rules. Interaction via the $\nu_4(b_1)$ mode is possible between the $^1B_1(\pi^*)$ and $^1A_1(3s)$ states ($B_1\otimes b_1\otimes A_1\supset A_1$) and between the $^1B_2(2p\text{-}2h)$ and $^1A_2(3d)$ states ($B_2\otimes b_1\otimes A_2\supset A_1$). In addition, there can be coupling of the $^1B_2(2p\text{-}2h)$ and $^1A_1(3s)$ states via the b_2 modes ν_5 or ν_6 ($B_2\otimes b_2\otimes A_1\supset A_1$).

TABLE VI. Intrastate vibronic coupling constants k_s (eV) for the lowest singlet C 1*s* excited states of H_2CO obtained at the MRCI level.

State	ν_1	ν_2	ν_3
$B_1(\pi^*)$	0.292	−0.205	0.055
$B_2(2p\text{-}2h)$	0.338	−0.451	0.106
$A_1(3s\text{-}a_1)$	0.058	0.010	−0.037

A. Determination of the LVC model parameters

For a more accurate and consistent treatment of the $^1B_1(\mathrm{C}\,1s\rightarrow\pi^*)$ and $^1A_1(\mathrm{C}\,1s\rightarrow 3s)$ singly excited states and the $^1B_2(\mathrm{C}\,1s,n\rightarrow\pi^{*2})$ double excitation, both the coupling constants (Tables VI and VII) and the transition energies (Table VIII) were deduced from MRCI results. The ground-state equilibrium geometry, the normal coordinates, and the vibrational frequencies were taken from a CCSD treatment of the H_2CO ground state (Table I). For the $^1A_2(3d)$ state, representing the upper electronic state in our model, the intrastate coupling constants were taken from the ADC(2) calculations while the interstate coupling constant corresponding to the interaction with the $^1B_2(2p\text{-}2h)$ state was extracted from the $^1B_2(2p\text{-}2h)$ PES according to Eq. (15).

For the κ_i^s constants of the $^1B_1(\pi^*)$ state the MRCI values agree very well with the ADC(2) results in Table II. Good agreement between the two methods is also seen for the κ_1 constants associated with the $^1B_2(2p\text{-}2h)$ and $^1A_1(3s)$ states. However, the κ_2 and κ_3 values for these states derived from the MRCI treatment are systematically smaller than the corresponding ADC(2) results. A similar observation can be made for the $^1B_1(\pi^*)$-$^1A_2(3d)$ interstate coupling constant. For the other interstate coupling constants λ_{ij}^s no ADC(2) values were generated because of the poor ADC(2) description of the $^1B_2(2p\text{-}2h)$ state. Among the two b_2 modes, only the ν_5 mode proved to be sufficiently active with respect to coupling of the $^1B_2(2p\text{-}2h)$ and $^1A_1(3s)$ states, and thus was included in the present model.

The magnitude of the interstate coupling constants for the states $^1B_1(\pi^*)$-$^1A_1(3s)$ and $^1B_2(2p\text{-}2h)$-$^1A_2(3d)$ (0.171 and 0.393, respectively) seems to suggest a relatively strong coupling of the respective PES. Nevertheless, the adiabatic energy surfaces of the $^1B_1(\pi^*)$ and $^1B_2(2p\text{-}2h)$ states resulting from these coupling parameters (see Ref. [16]) do not show the expected double minima. This suggests that for some reason the interstate coupling constants derived in the usual way using Eqs. (14) and (15) are too small. To improve the LVC model, an adjustment of the parameters to the actual physical situation is recommended here. To this end, a simple fitting procedure was performed, in which the λ_{ij}^s values were chosen in such a way that the MRCI stabilization energies for the $^1B_1(\pi^*)$ and $^1B_2(2p\text{-}2h)$ states at the ROHF stationary points [11] were reproduced. As seen in Table VII, the fitted λ_{ij}^s values (0.441 and 0.651, respectively) are substantially larger than the original MRCI values.

TABLE VII. Interstate vibronic coupling constants λ_s (eV) for the lowest singlet C 1*s* excited states of H_2CO obtained at the MRCI level, the ADC(2) level, and by a fitting procedure.

Interacting states		Mode	MRCI	ADC(2)	Fit
$B_1(\pi^*)$	$A_1(3s\text{-}a_1)$	$\nu_4(b_1)$	0.171	0.218	0.441
$B_2(2p\text{-}2h)$	$A_2(3d\text{-}a_2)$	$\nu_4(b_1)$	0.393[a]		0.651
$B_2(2p\text{-}2h)$	$A_1(3s\text{-}a_1)$	$\nu_6(b_2)$	0.053		

[a]Extracted from the lower surface according to Eq. (15).

TABLE VIII. Vertical Ω_v and adiabatic $\Omega_{0\text{-}0}$ transition energies for the lowest C 1*s* excited singlet states of H_2CO at the MRCI level, the minimal energies of conical intersection E_{int}, of the corresponding PES, and the energy gap Δ_{upp} (eV) between the intersection point and the adiabatic minimum of the upper surface.

State	Transition energy (eV)		$E_{\mathrm{int}}(\Delta_{\mathrm{upp}})$[a] (eV)	
	Ω_v	$\Omega_{0\text{-}0}$	$A_1(3s\text{-}a_1)$	$A_2(3d\text{-}a_2)$
$B_1(\pi^*)$	286.24	285.80	301.07 (10.72)	
$B_2(2p\text{-}2h)$	288.50	286.69	290.81 (0.47)	294.77 (2.14)
$A_1(3s\text{-}a_1)$	290.36	290.34		

[a]Derived from the present LVC model.

In Table IX we compare the geometrical parameters for the $^1B_1(\pi^*)$ and $^1B_2(2p\text{-}2h)$ states resulting from the adjusted LVC model with those from the full ROHF geometry optimization procedure [11]. For both states the stabilization energies and the out-of-plane angle are rather accurately reproduced by the LVC model. The LVC results for the remaining parameters are less satisfactory, though the general trend of changes with respect to the ground state is reproduced correctly. The only exception is the CH bond length in the $^1B_2(2p\text{-}2h)$ state, for which the present LVC model leads to an elongation instead of the expected contraction. This may be a consequence of the fact that the CO stretching mode ν_2 contains admixtures of CH stretching. The choice of a relatively large coupling constant for the ν_2 mode in order to reproduce the large CO bond elongation found at the ROHF level introduces also an increase of the CH bond length. The present MRCI energies of the $^1B_1(\pi^*)$, $^1B_2(2p\text{-}2h)$, and $^1A_1(3s)$ states differ by up to 0.4 eV from those reported in Ref. [11]. These discrepancies are due to different ground-state equilibrium conformations used in this work (CCSD level) and in the previous study (ROHF level). It should be noted that the adiabatic transition energies given here are the energies of the 0-0 transitions of the LVC model, whereas in Ref. [11] they were obtained from MRCI calculations at the ROHF final-state geometries.

B. LVC model computations

The vibronic spectra were computed using the model Hamiltonian [Eq. (7)] comprising the four lowest electronic states, $^1B_1(\pi^*)$, $^1B_2(2p\text{-}2h)$, $^1A_1(3s)$, and $^1A_2(3d)$, the three totally symmetric (a_1) modes $(\nu_1\text{-}\nu_3)$, and two nontotally symmetric modes, $\nu_4(b_1)$ and $\nu_5(b_2)$. The vibrational frequencies were taken from CCSD ground-state calculations. The choice of the intrastate and interstate coupling constants was as described in the preceding section.

TABLE IX. Structural parameters (bond lengths and angles) and stabilization energy E_s with respect to the planar (local maximum) configuration of H_2CO in the $^1B_1(\pi^*)$ and $^1B_2(2p\text{-}2h)$ C 1*s* excited states. The results are of a ROHF full geometry optimization [11] and of the present LVC model.

State	Method	R_{CO} (Å)	R_{CH} (Å)	∠H—C—H	ϕ[a]	E_s (eV)
$^1B_1(\pi^*)$	ROHF	1.297	1.010	119.4°	22.8°	0.006[b]
	LVC	1.280	1.032	116.6°	22.2°	0.005
$^1B_2(2p\text{-}2h)$	ROHF	1.390	1.015	107.8°	59.7°	0.344[b]
	LVC	1.371	1.179	100.6°	60.2°	0.341

[a]Angle between the bisector of the H_2C plane and the axis of the CO bond.
[b]MRCI calculation including Davidson correction performed for the optimal geometries found at the ROHF level [11].

It is interesting to inspect the conical intersections implied by the present LVC model. In Table VIII the minimal energies of the occurring conical intersections are listed. There is an intersection of the $^1B_2(2p\text{-}2h)$ and $^1A_1(3s)$ PES lying only 0.47 eV above the minimum of the $^1A_1(3s)$ surface. Thus, strong nonadiabatic effects can be expected in the $^1A_1(3s)$ excitation at energies close to and above this intersection. The $^1B_1(\pi^*)$ and $^1A_1(3s)$ PES, on the other hand, intersect at very high energy, namely at 10.7 eV above the minimum of the $^1A_1(3s)$ state. Clearly, this intersection has no significance for the nuclear dynamics in the corresponding transitions.

A basis-set representation of the vibronic model Hamiltonian was constructed using products of ground-state harmonic-oscillator states extending through 15, 50, 10, 80, and 30 quanta of the normal modes $\nu_1-\nu_5$, respectively. The computation of the vibronic spectrum, separately for the symmetry blocks A_1, B_1, and B_2 (each of dimension 10 800 000), was accomplished by performing 30 000 Lanczos iterations. After the diagonalization step the total theoretical photoabsorption spectrum was constructed according to Eq. (10) as the superposition of the individual spectra of the three vibronic symmetries. The electronic oscillator strengths for this step were taken from the ADC(2) calculations (Table II). For comparison with experiment, the constructed spectra were convoluted with Lorentzians of 0.14 eV FWHM. The general multistate vibronic coupling code written by two of us was used in these computations [33].

The resulting spectrum for the first two photoabsorption bands is shown in Fig. 3 in comparison with the recordings of Remmers *et al.* [2]. For the $^1B_1(\pi^*)$ and $^1A_1(3s)$ bands, a more detailed comparison of the LVC, PID, and experimental results are presented in Figs. 4 and 5. Figure 6 shows the LVC and PID results for the C $1s,n\rightarrow\pi^{*2}(^1B_2)$ transition.

C. The C $1s\rightarrow\pi^*(^1B_1)$ band

The main features of the C $1s\rightarrow\pi^*(^1B_1)$ photoabsorption band [Fig. 4(a)] are well reproduced already at the PID level [Fig. 4(b)], although the experimental spectrum looks somewhat more diffuse. As mentioned in Sec. III A, the vibrational pattern here is dominated by excitations of the ν_2 and ν_1 modes. As seen from the comparison of the PID and the experimental results, all major features in the experimental spectrum can be explained by the excitations of these two modes, in agreement with the conclusions of Remmers *et al.* [2]. More specifically, the first four peaks resolved in experiment can be attributed to 0-0, 2^1_0, $1^1_0+2^1_0$, $1^1_0\,2^1_0$ transitions, respectively. There are small discrepancies with respect to the intensity distribution, in particular the intensity maximum of the PID is seen to be shifted to a lower member of the vibrational progression. This indicates that the present intrastate coupling constants κ_1 and κ_2 might be underestimated. Moreover, the experimental frequency of the ν_2 mode [2] is by factor of 1.4 smaller than the ν_2 frequency in the

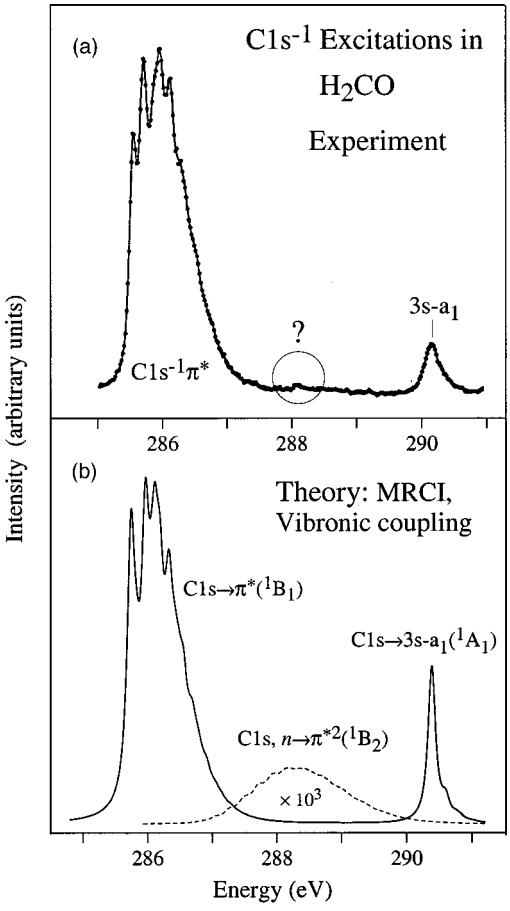

FIG. 3. C 1*s* photoabsorption below 291 eV. (a) Experiment [2]. (b) Theoretical vibronic coupling spectrum obtained from MRCI excitation energies and vibronic coupling constants (Tables VI and VII).

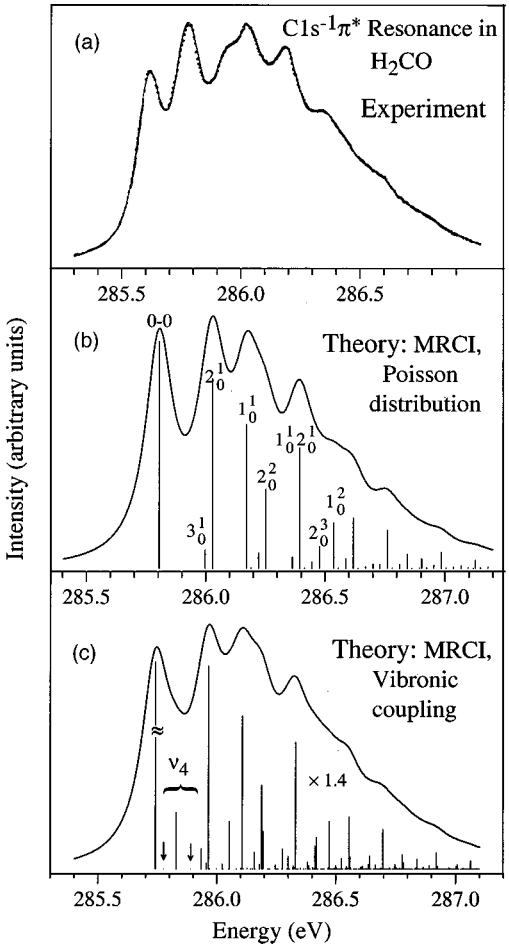

FIG. 4. C $1s\rightarrow\pi^*$ ($^1B_1$) photoabsorption band. (a) Experimental spectrum [2]. (b) Theoretical curve at the Poisson intensity distribution level. (c) Result of the multistate vibronic coupling model (Sec. IV).

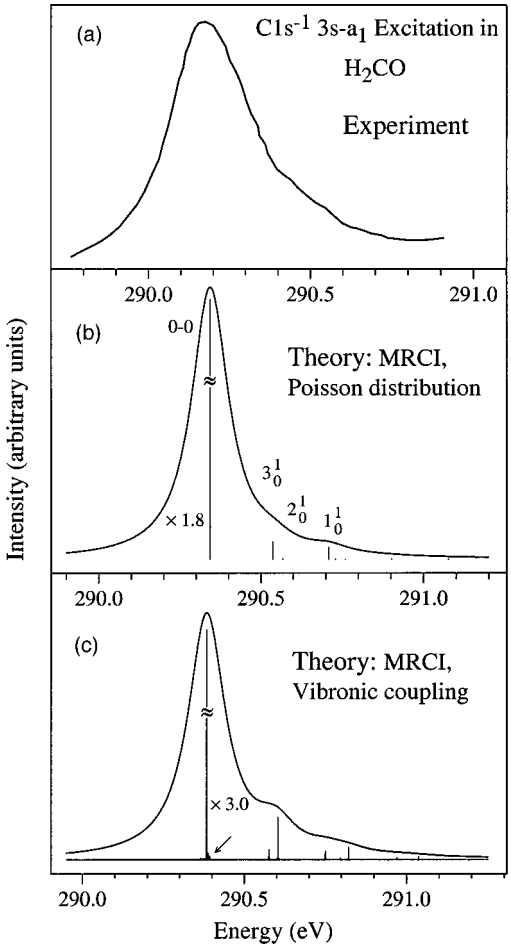

FIG. 5. C $1s\rightarrow 3s(^1A_1)$ photoabsorption band. (a) Experimental spectrum [2]. (b) Theoretical curve at the Poisson intensity distribution level. (c) Result of the multistate vibronic coupling model (Sec. IV).

electronic ground state used in the PID spectrum, which gives rise to some disagreement with respect to the spacing of the vibrational peaks.

Turning to the results of our LVC calculations in Fig. 4(c), one immediately sees that density of states in the vibronic spectrum is distinctly increased compared to the PID spectrum. This leads to a somewhat broadened spectral envelope and to less symmetric shapes of the individual peaks. In addition to the pattern formed by the strong ν_2 and ν_1 vibrations there appear many weak lines, some of them already at quite low excitation energy. These new lines are clearly related to the excitation of the out-of-plane bending mode ν_4, a finding consistent with the double minimum on the $^1B_1(\pi^*)$ PES. According to the present results, the frequency of the ν_4 mode in the $^1B_1(\pi^*)$ state is reduced to about 712 cm^{-1} with respect to the ground-state value of 1167 cm^{-1} [2].

The presence of the ν_4 excitations in the low-energy region of the π^* band can explain the puzzling alternation of the spectral shape upon deuteration observed by Remmers *et al.* [2]. According to the Franck-Condon analysis of these authors, an isotopic effect should not be expected here, since this spectral region is dominated by the excitation of the CO stretching mode ν_2. Our LVC calculations, however, show clearly that the spectral part below 286 eV contains substantial contributions of excitations of the out-of-plane bending mode ν_4 (note the strong ν_4 line between the 0-0 and 2^1_0 lines in Fig. 4(c).

Since the frequency of the ν_4 mode changes considerably upon deuteration (from 1167 to 938 cm^{-1} in the electronic ground state) [2], our results imply that indeed an isotopic effect must be expected in the low-energy part of the π^* band.

D. The C $1s\rightarrow 3s$-$a_1(^1A_1)$ band

The experimental C $1s\rightarrow 3s$-$a_1(^1A_1)$ band is a broad hump with a shoulder on the high-energy side, showing no sign of resolved vibrational structure [Fig. 5(a)]. The experimental width of this band (0.24 eV) [2] is much larger than the average linewidth of the C $1s$ excitations (0.12–0.16 eV). There is a pronounced isotopic effect upon deuteration [2], resulting in a smaller width and a positive energy shift of the maximum. Since the $3s$-a_1 band is believed to be mainly due to the 0-0 transition [2], the observed irregularities cannot readily be explained. The suggestion made in Ref. [2]

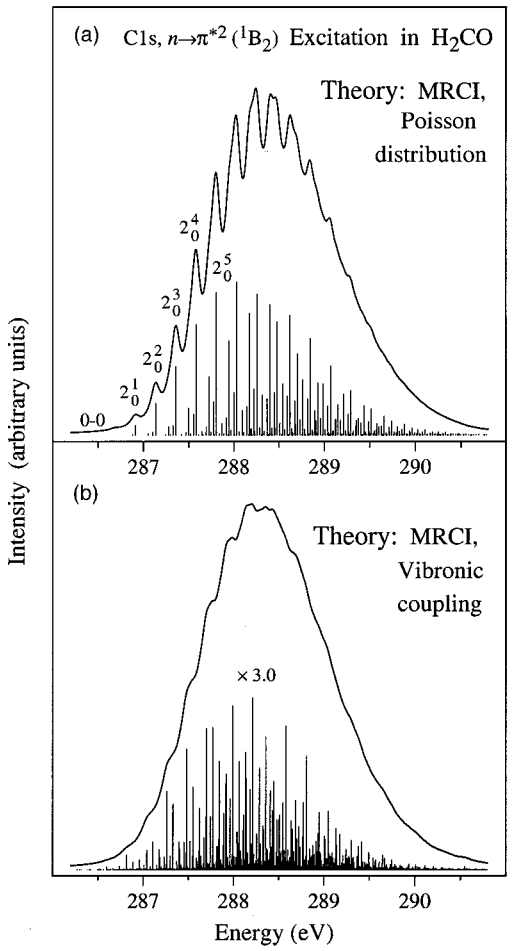

FIG. 6. Theoretical C $1s,n\rightarrow\pi^{*2}(^1B_2)$ transition spectra. (a) Poisson intensity distribution. (b) Result of the multistate vibronic coupling model (Sec. IV).

that there is a perturbation of the $^1A_1(3s)$ Rydberg state by ''molecular orbitals'' and to ''a breakdown of the Born-Oppenheimer approximation'' seems intuitively correct, but certainly the reasoning should be based on the more stringent grounds of a vibronic coupling study as is attempted here. In agreement with Remmers *et al.* [2], our PID results [Fig. 5(b)] confirm the dominating role of the 0-0 transition in the $3s$-a_1 band. Two much weaker lines seen in the PID spectrum at higher energy are the excitations 3_0^1 and 1_0^1, respectively. They are clearly related to the high-energy shoulder in the experimental spectrum, though their intensity relative to the 0-0 line appears to be somewhat underestimated. Moreover, the large width of the experimental peak is not reproduced by the PID results.

The observed broadening of the $3s$-a_1 band suggests the presence of a fast decay channel for the $^1A_1(3s)$ state. One possibility for such a process might arise from vibronic coupling between the $^1A_1(3s)$ state and the lower-lying $^1B_1(\pi^*)$ and $^1B_2(2p$-$2h)$ states, allowing for a ''decay'' of the totally symmetric vibrational levels of the $^1A_1(3s)$ state into the dense quasicontinuum of nontotally symmetric vibrational levels of the $^1B_1(\pi^*)$ and $^1B_2(2p$-$2h)$ states. Another possibility follows from our previous work [11], showing that the $^1A_1(3s)$ state is locally bound, but thermodynamically unstable with respect to the dissociation into O (^3P) and C $1s$ excited $CH_2(^3B_2)$. This means that the discrete vibrational levels of the $^1A_1(3s)$ state are embedded in the continuum of dissociative states. Of course, both of the latter two decay channels of the $^1A_1(3s)$ state may contribute to the observed broadening. However, a modest broadening effect due to vibronic coupling can readily be seen in our vibronic spectrum [Fig. 4(c)]. The effective width of the 0-0 transition is about 10% larger than in the PID result. The broadening is the result of an accumulation of many weak lines (satellites) in the vicinity of the totally symmetric vibrational transitions. In particular, the 0-0 line itself is split into several close components, not visible in Fig. 5(c). The intensity of the satellites drops with the distance from the main transition, but never reaches zero: the contiguous line at the bottom of Fig. 5(c) was generated by plotting the satellite bar spectrum. Since the larger part of the $3s$-a_1 band lies below the energy of the conical intersection point at about 290.8 eV, most features show a one-to-one correspondence with those of the PID spectrum. Apart from the effect of line splitting, the LVC spectrum shows a substantial increase of the 2_0^1 line as an effect of intensity borrowing, leading to a better agreement of the theoretical and experimental spectral profiles.

Since the experimental width of the $3s$-a_1 band could not be reproduced by our vibronic calculations, the source of the broadening must be sought in the dissociation processes. This is quite consistent with the experimental findings, especially with the linewidth reduction upon deuteration. The origin of the positive-energy shift of the band maximum, however, remains unclear. Here a more rigorous treatment of the resonance-type interaction between the discrete $^1A_1(3s)$ levels and the dissociative continuum is desirable.

E. The C $1s,n\rightarrow\pi^{*2}(^1B_2)$ band

Because of its very small optical intensity predicted by our calculations, the C $1s,n\rightarrow\pi^{*2}(^1B_2)$ transition cannot be seen in the theoretical vibronic spectrum [Fig. 3(b)]. The contribution of the B_2 vibronic symmetry (displayed with an amplification factor of 10^3) has an intensity maximum near 288.3 eV, which is just in between the π^* resonance and the $3s$-a_1 band. Although here the spectral intensity of the latter bands is very small, the C $1s,n\rightarrow\pi^{*2}(^1B_2)$ transition is completely covered up. Of course, the question of the observation of the C $1s,n\rightarrow\pi^{*2}(^1B_2)$ transition in optical spectroscopy depends crucially on the actual magnitude of the corresponding oscillator strength. It may well be that the ADC(2) value is too small. Nooijen and Bartlett [4] find an absolute f value of 3.9×10^{-4}, which is about 40 times larger than the present ADC(2) value of 1×10^{-5}.

The PID and LVC spectra of the C $1s,n\rightarrow\pi^{*2}(^1B_2)$ transition, displayed in Fig. 6, give a detailed insight into the role of the vibronic coupling effect. In the PID spectrum [Fig. 6(a)] the vibrational progression is dominated by the excitations of the ν_2 mode, which together with excitations of the ν_1 mode shape the overall appearance of the band. A similar pattern of totally symmetric excitations can still be seen in

the LVC spectrum, but here many additional ν_4 excitations give rise to an extremely dense and complex line structure. As a result, the structured Poisson spectrum is transformed into a fairly smooth curve, preserving essentially the original PID envelope. As a further broadening mechanism not covered by the present vibronic model the possibility of dissociation should be kept in mind. This is suggested by Ref. [11] predicting that the vertical transition to the $^1B_2(2p\text{-}2h)$ state should populate the unbound part of the PES.

Since the $^1B_2(2p\text{-}2h)$ state is coupled via the ν_5 vibrational mode to the $^1A_1(3s)$ state, the possibility of an intensity borrowing between the more intense C $1s \rightarrow 3s\text{-}a_1(^1A_1)$ transition and the C $1s,n \rightarrow \pi^{*2}(^1B_2)$ transition was suggested in Ref. [11], which could eventually make the latter transition observable in the photoabsorption spectrum. However, according to the present results this intensity borrowing effect appears to be rather small and not sufficient to render this state visible. The origin of the small, barely visible bump in the experimental spectrum [2] near 288.1 eV (designated with the question mark in Fig. 3(a)) and its possible relation to the $^1B_2(2p\text{-}2h)$ therefore still remains an open issue. It should be noted, however, that possibly the interstate coupling constant λ_{ij}^s, coupling the $^1A_1(3s)$ and $^1B_2(2p\text{-}2h)$ states via the ν_2 mode, is too small, leading to an underestimation of the intensity borrowing effect.

V. CONCLUDING REMARKS

In the present study of C $1s$ and O $1s$ excitations in the prototypical H_2CO molecule we have combined *ab initio* quantum-chemical computations of electronic excitation energies and oscillator strengths with a treatment of the vibrational excitation accompanying the electronic transitions. The resulting theoretical spectral profiles are in very good agreement with the high-resolution photoabsorption spectra recorded by Remmers *et al.* [2], allowing for a more detailed understanding of the experimental findings.

While for the C $1s$ excitations the present results support essentially the previous assignments [1–5], the interpretation of the O $1s$ Rydberg spectrum has to be revised: here, according to our study, the dominating spectral contributions are due to *nd* rather than to *np* Rydberg transitions. The reason is the partial localization of the lowest *np* Rydberg orbitals at the carbon site of the molecule, leading to a suppression of the O $1s\text{-}np$ oscillator strengths.

The vibrational excitation pattern of most electronic transitions is qualitatively well described already by the simple Poisson intensity distribution [16], predicting correctly the vibrational activity of the three totally symmetric modes, $\nu_1 - \nu_3$. There are, however, distinct effects induced by vibronic coupling, as our four-state five-mode LVC model for the lowest C $1s$ excitations reveals. In the case of the C $1s \rightarrow \pi^*(^1B_1)$ excitation, this coupling leads to a more complex spectral profile, reflecting in particular a strong excitation of the ν_4 out-of-plane bending mode already in the low-energy part of the band. The presence of these low-lying CH_2 bending vibrations explain in a natural way the marked isotopic effect observed by Remmers *et al.* [2] in this part of the spectrum.

A more complicated physical situation is found for the case of the C $1s \rightarrow 3s(^1A_1)$ band, where several possibly competing decay mechanisms lead to the appearance of a broad, almost structureless hump. Apart from the electronic Auger decay, a source of broadening is vibronic coupling with the energetically lower $^1B_1$ (C $1s \rightarrow \pi^*$) and $^1B_2(2p\text{-}2h)$ states, considered in our multistate vibronic coupling model. According to the present results, however, this effect is relatively modest and cannot explain the observed broadening. Most likely, the dissociation reaction $H_2CO^*(^1A_1) \rightarrow CH_2^*(^3B_1) + O(^3P)$ is the decay channel responsible for the large width and the unusual isotopic effect of the C $1s \rightarrow 3s(^1A_1)$ band (see Ref. [11]). A final clarification of this issue must be deferred to future experimental and theoretical studies.

Another finding not clarified by the present study is the diffuse appearance of the O $1s$ spectral bands. According to our PID treatment, vibrational structure should be discernible for the O $1s \rightarrow \pi^*(^1B_1)$ band, as well as for several of the O $1s$ Rydberg transitions.

An interesting aspect of the *K*-shell spectroscopy of H_2CO is the different behavior of the CO bond length in C $1s$ and O $1s$ Rydberg excitations, leading to a decrease in the former and an increase in the latter case. This could be rationalized by discussing the bond-length dependence of the correlation-induced intramolecular charge transfer in the H_2CO ground state. The increase of the CO bond length leads to a decrease of the charge at the carbon site, which means antiscreening for the C $1s$ orbital and, thus, an increase of the energy needed to remove an electron from the C $1s$ orbital. The opposite situation applies to the case of O $1s$ excitation.

Another example for the importance of core-hole screening is the presence of the energetically low $^1B_2$ (C $1s,n \rightarrow \pi^{*2}$) double excitation at about 288.3 eV, that is, being placed second in the C $1s$ excitation spectrum. Here the C $1s$-hole screening arises from the intramolecular charge transfer due to the $n \rightarrow \pi^*$ valence-electron promotion. The transition has very low intensity, making it hardly observable in optical spectroscopy. The possibility of an efficient intensity borrowing effect via vibronic interaction with the $^1A_1$ (C $1s \rightarrow 3s$) state could not be confirmed by our LVC model calculations. As discussed in Ref. [11], better chances for the experimental detection of this state should be offered by resonant photoemission. The present example of a low-lying double excitation suggests that one may find *K*-shell double excitations even below the first single excitation in molecules with sufficiently strong charge-transfer valence-electron excitations.

ACKNOWLEDGMENTS

The authors are indebted to Dr V. B. Kobichev for useful discussions. One of the authors (A.B.T.) gratefully acknowledges support from the Alexander von Humboldt foundation. This work has been supported by the Deutsche Forschungsgemeinschaft (DFG).

[1] A. P. Hitchcock and C. E. Brion, J. Electron Spectrosc. Relat. Phenom. **19**, 231 (1980).
[2] G. Remmers, M. Domke, A. Puschmann, T. Mandel, C. Xue, G. Kaindl, E. Hudson, and D. A. Shirley, Phys. Rev. A **46**, 3935 (1992).
[3] J. Schirmer, A. Barth, and F. Tarantelli, Chem. Phys. **122**, 9 (1988).
[4] M. Nooijen and R. J. Bartlett, J. Chem. Phys. **102**, 6735 (1995).
[5] G. Fronzoni, M. Stener, A. Lisini, and P. Decleva, Chem. Phys. **210**, 447 (1996).
[6] M. Domke, C. Xue, A. Puschmann, T. Mandel, E. Hudson, D. A. Shirley, and G. Kaindl, Chem. Phys. Lett. **173**, 122 (1990); **174**, 668 (1990); Y. Ma, C. T. Chen, G. Meigs, K. Randall, and F. Sette, Phys. Rev. A **44**, 1848 (1991); E. Shigemasa, T. Hayaishi, T. Sasaki, and A. Yagishita, *ibid.* **47**, 1824 (1993).
[7] C. T. Chen, Y. Ma, and F. Sette, Phys. Rev. A **40**, 6737 (1989); E. Shigemasa, K. Ueda, Y. Sato, T. Sasaki, and A. Yagishita, *ibid.* **45**, 2915 (1992).
[8] J. Schirmer, A. B. Trofimov, K. J. Randall, J. Feldhaus, A. M. Bradshaw, Y. Ma, C. T. Chen, and F. Sette, Phys. Rev. A **47**, 1136 (1993).
[9] F. X. Gadea, H. Köppel, J. Schirmer, L. S. Cederbaum, K. J. Randall, A. M. Bradshaw, Y. Ma, F. Sette, and C. T. Chen, Phys. Rev. Lett. **66**, 883 (1991); B. Kempgens, B. S. Itchkawitz, K. J. Randall, J. Feldhaus, A. Bradshaw, H. Köppel, F. X. Gadea, D. Nordfors, J. Schirmer, and L. S. Cederbaum, Chem. Phys. Lett. **246**, 347 (1995); H. Köppel, F. X. Gadea, G. Klatt, J. Schirmer, and L. S. Cederbaum, J. Chem. Phys. **106**, 4415 (1997).
[10] M. Neeb, A. Kivimäki, B. Kempgens, H. M. Köppe, J. Feldhaus, and A. M. Bradshaw, Phys. Rev. Lett. **76**, 2250 (1996); H. M. Köppe, B. Kempgens, A. L. D. Kilcoyne, J. Feldhaus, and A. M. Bradshaw, Chem. Phys. Lett. **260**, 223 (1996); M. N. Piancastelli, A. Kivimäki, B. Kempgens, M. Neeb, K. Maier, and A. M. Bradshaw, *ibid.* **274**, 13 (1997).
[11] A. B. Trofimov, E. V. Gromov, T. E. Moskovskaya, and J. Schirmer, J. Chem. Phys. **113**, 6716 (2000).
[12] J. Schirmer, Phys. Rev. A **26**, 2395 (1982).
[13] A. B. Trofimov and J. Schirmer, J. Phys. B **28**, 2299 (1995).
[14] A. Barth and J. Schirmer, J. Phys. B **18**, 867 (1982).
[15] A. B. Trofimov, T. E. Moskovskaya, E. V. Gromov, N. M. Vitkovskaya, and J. Schirmer, J. Struct. Chem. **41**, 590 (2000).
[16] H. Köppel, W. Domcke, and L. S. Cederbaum, Adv. Chem. Phys. **57**, 59 (1984).
[17] J. Schirmer and F. Mertins, Int. J. Quantum Chem. **58**, 329 (1996).
[18] L. S. Cederbaum, W. Domcke, and J. Schirmer, Phys. Rev. A **22**, 206 (1980).
[19] W. Lichten, Phys. Rev. **131**, 229 (1963); Phys. Rev. **139**, A27 (1965); Phys. Rev. **164**, 131 (1967); F. T. Smith, Phys. Rev. **179**, 111 (1969); T. F. O'Malley, Adv. At. Mol. Phys. **7**, 223 (1971); T. Pacher, L. S. Cederbaum, and H. Köppel, Adv. Chem. Phys. **84**, 293 (1993).
[20] L. S. Cederbaum and W. Domcke, Adv. Chem. Phys. **36**, 205 (1977).
[21] J. Cullum and R. Willoughby, *Lanczos Algorithm for Large Symmetric Eigenvalue Problems* (Birkhäuser, Boston, 1985), Vols. I and II.
[22] E. B. Wilson, Jr., J. C. Decius, and P. C. Cross, *Molecular Vibrations* (McGraw-Hill, New York, 1955).
[23] S. Huzinaga, J. Chem. Phys. **42**, 1293 (1965).
[24] T. H. Dunning, Jr., J. Chem. Phys. **90**, 1007 (1989).
[25] K. Kaufmann, W. Baumeister, and M. Jungen, J. Phys. B **22**, 2223 (1989).
[26] M. J. Frisch, G. W. Trucks, H. B. Schlegel, G. E. Scuseria, M. A. Robb, J. R. Cheeseman, V. G. Zakrzewski, J. A. Montgomery, Jr., R. E. Stratmann, J. C. Burant, S. Dapprich, J. M. Millam, A. D. Daniels, K. N. Kudin, M. C. Strain, O. Farkas, J. Tomasi, V. Barone, M. Cossi, R. Cammi, B. Mennucci, C. Pomelli, C. Adamo, S. Clifford, J. Ochterski, G. A. Petersson, P. Y. Ayala, Q. Cui, K. Morokuma, D. K. Malick, A. D. Rabuck, K. Raghavachari, J. B. Foresman, J. Cioslowski, J. V. Ortiz, A. G. Baboul, B. B. Stefanov, G. Liu, A. Liashenko, P. Piskorz, I. Komaromi, R. Gomperts, R. L. Martin, D. J. Fox, T. Keith, M. A. Al-Laham, C. Y. Peng, A. Nanayakkara, C. Gonzalez, M. Challacombe, P. M. W. Gill, B. Johnson, W. Chen, M. W. Wong, J. L. Andres, C. Gonzalez, M. Head-Gordon, E. S. Replogle, and J. A. Pople, GAUSSIAN 98, Revision A.7, Gaussian, Inc., Pittsburgh, PA, 1998.
[27] D. J. Cloutier and D. A. Ramsey, Annu. Rev. Phys. Chem. **34**, 31 (1983).
[28] G. Schaftenaar and J. H. Noordik, J. Comput.-Aided Mol. Des. **14**, 123 (2000).
[29] M. W. Schmidt, K. K. Baldridge, J. A. Boatz, S. T. Elbert, M. S. Gordon, J. H. Jensen, S. Koseki, N. Matsunaga, K. A. Nguyen, S. Su, T. L. Windus, M. Dupuis, and J. A. Montgomery, Jr., J. Comput. Chem. **14**, 1347 (1993).
[30] V. R. Saunders and J. H. van Lenthe, Mol. Phys. **48**, 923 (1983).
[31] Program written by M. F. Guest, J. H. van Lenthe, J. Kendrick, K. Schoffel, and P. Sherwood, with contributions from R. D. Amos, R. J. Buenker, M. Dupuis, N. C. Handy, I. H. Hiller, P. J. Knowles, V. Bonacic-Koutecky, W. von Niessen, R. J. Harrison, A. P. Rendell, V. R. Saunders, and A. J. Stone. The package is derived from the original GAMESS code due to M. Dupuis, D. Spangler, and J. Wendoloski, NRCC Software Catalog, Vol. 1, Program No. QG01 (GAMESS), 1980.
[32] C. L. Pekeris, Phys. Rev. **112**, 1649 (1958).
[33] Program written by A. B. Trofimov and E. V. Gromov, Irkutsk State University, 1999.